Available online at www.sciencedirect.com
SCIENCE DIRECT®
International Journal of Heat and Mass Transfer 47 (2004) 2551–2565
International Journal of HEAT and MASS TRANSFER
www.elsevier.com/locate/ijhmt

Effect of axial conduction on the heat transfer in micro-channels

I. Tiselj [a], G. Hetsroni [b,*], B. Mavko [a], A. Mosyak [b], E. Pogrebnyak [b], Z. Segal [b]

[a] "Jozef Stefan" Institute, Jamova 39, 1000 Ljubljana, Slovenia
[b] Department of Mechanical Engineering, Technion—Israel Institute of Technology, Haifa 32000, Israel

Received 9 June 2003; received in revised form 5 January 2004

Abstract

Experimental and numerical analysis were performed to evaluate heat transfer characteristics of water flowing through triangular silicon micro-channels with hydraulic diameter of 160 μm in the range of Reynolds number $Re = 3.2$–64. It was shown that as the bulk water temperature, as well as the temperature of the heated wall, do not change linearly along the channel. The experimental results of temperature distribution on the heated wall agree with the numerical predictions.

The behaviour of the Nusselt number along the channel has a singular point. At this point, the difference between the temperatures on the wall and the bulk water becomes negative and the flux changes the sign and is directed from the fluid to the wall. The singular point shifts closer to the channel outlet with an increase of the Reynolds number.

It was shown that under conditions of the present study the heat transfer may be described by conventional Navier–Stokes and energy equations as a common basis.

Keywords: Convective heat transfer; Micro-channels; Fluid flow; Axial heat conduction

1. Introduction

Among the novel methods for thermal management of power modules of micro-electronic devices, micro-channels are the most effective at heat removal. Many correlations have been proposed in the literature for heat transfer, based on experimental investigations on liquid and gas flow in mini- and micro-channels. Sobhan and Garimella [1] presented a comprehensive review of these investigations conducted over the past decade.

Many experimental studies have shown departure from the conventional theory for heat transfer. Choi et al. [2] found that measured Nusselt number in laminar flow exhibits a Reynolds number dependence, in contrast to the conventional prediction for fully developed laminar flow, in which Nusselt number is constant. The heat transfer at forced convection in channels with cross-section of 0.6×0.7 mm was experimentally investigated by Peng and Wang [3]. They showed that the dependence of the Nusselt number on the Reynolds number exhibited an unusual tendency. Weisberg et al. [4] and Bowers and Mudawar [5], also noted that behaviour of fluid flow and heat transfer in micro-channels without phase change is substantially different from that which typically occurs in conventionally sized channels. Wang and Peng [6] reported single-phase heat transfer coefficients in six rectangular channels having $0.31 < d_h < 0.75$ mm for water and methanol. The Nusselt numbers were only 35% of those predicted by the Dittus–Boetler equation. However, Webb and Zhang [7] found that their experimental results were adequately predicted by the commonly

* Corresponding author. Tel.: +972-4-8292058; fax: +972-4-8238101.
E-mail address: hetsroni@techunix.technion.ac.il (G. Hetsroni).

0017-9310/$ - see front matter © 2004 Elsevier Ltd. All rights reserved.
doi:10.1016/j.ijheatmasstransfer.2004.01.008

Nomenclature

$\dot{m}$	mass flow rate
a	base of the triangular channel
A	heated area
C_p	specific heat
d	diameter
F	cross-section area
h	heat transfer coefficient
I	current
k	thermal conductivity
L	length of the module
N	power
$Nu = hd_h/k$	Nusselt number
p	pressure
Pr	Prandtl number
q	heat flux
Q	volumetric flow rate
$Re = ud_h/v$	Reynolds number
T	temperature
u	velocity
V	voltage
z, x, y	axial, transverse, vertical co-ordinates, respectively

Greek symbols

α	thermal diffusivity
ρ	density
v	kinematic viscosity

Subscripts

a	ambient
c	cross-section
f	fluid
h	hydraulic
in	inlet
l	losses
out	outlet
p	pyrex
s	solid
th	thermal

accepted correlations for single-phase flow in multiple tubes having hydraulic diameters between 0.96 and 2.1 mm. Wu and Little [8] measured the flow and heat transfer characteristics for the flow of nitrogen gas in heat exchangers. The Nusselt numbers for laminar flow ($Re < 600$) were lower than those predicted by correlations. Peng and Peterson [9] showed a strong effect of geometric configuration (aspect ratio and the ratio of the hydraulic diameter to the center-to-center distance of the micro-channels) on the heat transfer and flow characteristics in single-phase laminar flow. Qu et al. [10] reported that the experimentally determined Nusselt number in the laminar regime is lower than that predicted by the numerical analysis. There is no conclusive explanation of these observations up to now, although some physical phenomena (surface roughness, coupling between momentum transfer and conduction heat transfer in the liquid, natural convection, etc.) have been suggested to interpret these deviations from the heat transfer laws in large-scale channels.

A roughness-viscosity model was applied by Qu et al. [10] to explain the experimental results. They assumed that the velocity gradient near the wall was reduced because of the roughness, the temperature gradient near the wall was also reduced, and hence, the convective heat transfer was also reduced. According to Qu et al. [10] that might be the reason why the experimental Nusselt number is smaller than the numerical result of the conventional heat transfer theory. The low Nusselt numbers in laminar flow were attributed by Tso and Mahulicar [11,12] to the Brinkman number, Br, which represents the ratio of the heat transferred from the wall by fluid conduction along the micro-channel to the work done against viscous shear. The Brinkman number is a measure of the effect of viscous dissipation relative to the heat transferred by conduction. The authors reported that the introduction of this parameter into consideration, in addition to Reynolds and Prandtl numbers, could explain the unusual behaviour of convective heat transfer in the laminar regime in micro-channels.

Some authors provide experimental and numerical results for water flow in micro-channels in agreement with predicted values for the friction factor and Nusselt number. The experimental and numerical study of pressure drop and heat transfer in a single-phase micro-channel heat sink carried out by Qu and Mudawar [13,14] demonstrated that the conventional Navier–Stokes and energy equations can adequately predict the fluid flow and heat transfer characteristics of micro-channel heat sinks.

New questions have arisen in micro-scale flow and heat transfer. These problems have been considered in several review papers by Gad-el-Hak [15], Mehendale et al. [16] and Palm [17]. The review by Gad-el-Hak [15] focused on the physics related to the breakdown of the N–S equations. Mehendale et al. [16] thought that since the heat transfer coefficients were based on the inlet and/or outlet fluid temperatures, not the bulk temperatures in almost all studies, comparison of conventional correlations is problematic. Palm [17] also suggested several possible explanations for the variations of micro-scale single-phase heat transfer from convectional theory, including surface roughness effects and entrance effects.

On the other hand, there is a significant difference between experimental measured Nusselt numbers by Tso

and Mahulikar [12] and calculations carried out by Herwig and Hausner [18], with flow and thermal boundary conditions of the experiments in [12]. In experiments Nusselt numbers were between 1 and 2 for Reynolds number about 50, whereas calculated Nusselt number was close to 4.36.

It should be noted, that in experimental investigations of heat transfer in micro-tubes [11–14] the axial heat flux was not measured. In general, the axial heat conduction in the channel wall, for conventional size channels, can be neglected because the wall thickness is usually very small compared to the channel diameter. Shah and London [19] found that the Nusselt number for developed laminar circular pipe flow is between 4.36 and 3.66, which correspond to Nusselt numbers for constant heat flux and constant temperature boundary conditions, respectively. A three-dimensional model was developed by Fedorov and Viskanta [20] to investigate flow and conjugate heat transfer in the micro-channel. The detailed temperature and heat flux distribution, as well as the average heat transfer characteristics, are reported for channels of hydraulic diameter 86 μm. The wall temperatures increased drastically in the longitudinal distance within the small inlet portion of the channel ($z/L < 0.1$) and then did not change. On the other hand, Qu and Mudawar [14] demonstrated that a linear temperature rise is a good approximation for the behaviour of wall temperature. It is clear that predictions of the local temperature and heat fluxes are depended on the heat sink design, specific flow and heat transfer conditions.At this time, there is a wide gap between experimental and numerical results. That is why this study was carried out.

This study focuses on the effect of axial heat flux on heat transfer in micro-channel for low Reynolds numbers. For this, an experimental module was built and a systematic study was done to determine the values of the axial heat flux. These data were used for validation of numerical calculations. A discussion of these results is developed and allows the analysis of the Nusselt number variation in parallel triangular micro-channels connected by common collectors.

2. Experimental set-up and procedure

Experimental facility. The experimental facility and flow loop, are described in detail in [21,22]. The loop consists of a liquid peristaltic pump, piping, test module, entrance and exit tanks. Working liquid was pumped from the entrance tank through the inlet collector to the micro-channels in the test module, and from the micro-channels through the outlet collector to the exit tank.

The temperature of the working fluid was measured at the inlet and outlet collector of the test module, by 0.3 mm type-T thermocouples. The thermocouples were calibrated using the Model 9100 HDRC Handheld Dry-well calibrator in 0.1 K increments. The flow rate of the working fluid was measured with an accuracy of 0.5%. The data were collected by a data acquisition system.

Test module. The test module, Fig. 1, was fabricated of a square-shape silicon substrate 15×15 mm, 530 μm thick, and utilised a Pyrex cover, 500 μm thick, which served as both an insulator and a transparent cover through which flow in micro-channels could be observed. In the silicon substrate, seventeen parallel micro-channels were etched. The cross-section of each channel is an isosceles triangle with a base of $a = 310$ μm. The angles at the base are 55°. An electrical heater of 10×10 mm^2, made of a thin film resistor, had been deposited on the surface of the silicon, and served to simulate the heat source. The heater has serpentine pattern as shown in Fig. 1. The heater filament has a dimension of 0.001 mm in thickness, 0.2 mm in width and 250 mm in length. This design allows a uniform heating of the surface and reduces the contact resistance between the heater and the wafer. To estimate the contact resistance between the heater and the wafer the resulting heat flux through the inclined wall of the channel was calculated and compared to the input heat flux. Convergence of the solution was assumed when the difference between the two fluxes was less than 0.1% [22]. It was shown that for the heat flux of 36 kW/m^2 the temperature of the channel wall is about 0.25 K lower than the measured temperature on the heater. This small temperature difference is a result of the low thermal resistance between the heater and the

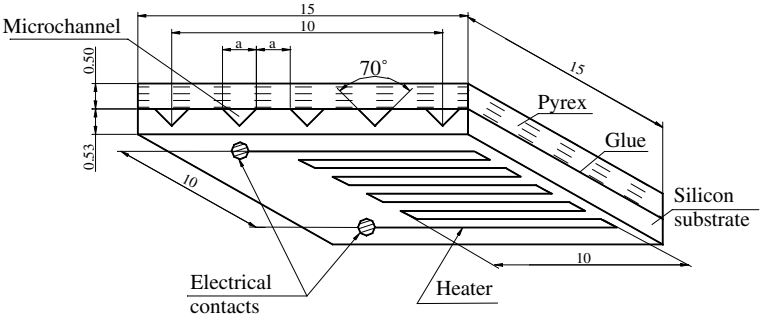

Fig. 1. Scheme and geometry of the silicon chip.

wafer, high thermal conductivity of the silicon and small thickness of the die. Taking into account that thermal resistance of the silicon substrate was 3.6×10^{-6} m^2 K/W we estimated the contact thermal resistance of the heater about 3.4×10^{-6} m^2 K/W.

The test module was connected to inlet and outlet manifolds. The input voltage and current were controlled by a power supply and measured with an accuracy of 0.5%. A thermal imaging radiometer was used to study the temperature field on the electrical heater. Its recording rate was 25 frames per second, with a resolution of 256 pixels per line and typical minimum detectable temperature difference of 0.1 K. The instantaneous field of view was 1.8 mrad.

For a normal testing procedure, the pump was turned on and the electrical power to the heater was adjusted to a desired level by a variable voltage controller. The module was then allowed to reach a steady state, which was achieved within 4–5 min from the moment the flow conditions were stabilised.

Data reduction. The parameters used in the data reduction and analysis are summarized below:

The total heat input to the silicon wafer may be expressed as

$$N = N_1 + N_2 + N_3 \tag{1}$$

where N is the Joule heating in the heater, N_1 is the power transferred to the fluid in the channels, N_2 is the power conducted through the silicon wafer in the axial direction, N_3 is the power dissipated due to heat losses.

The power generated by Joule heating in the heater was

$$N = IV \tag{2}$$

where I and V are the input current and voltage.

The power transferred to the fluid was estimated as

$$N_1 = \dot{m}C_p(T_{\mathrm{f,out}} - T_{\mathrm{f,in}}) \tag{3}$$

where $\dot{m}$ is the mass flow rate, C_p is specific heat, $T_{\mathrm{f,in}}$ and $T_{\mathrm{f,out}}$ are the inlet and outlet water temperatures measured at the inlet and outlet collector, respectively. However, the numerical simulations described in the next section, show that this is not very accurate approximation, because of the significant temperature gradients in the inlet and outlet collectors. The temperature at the entrance (exit) of the channels can be a few degrees different than the temperature in the center of the inlet (outlet) collector, where the water temperatures were measured. Thus the Eq. (3) is only a rough estimate of the N_1 power.

For each set of steady-state experimental conditions the energy balance (based on the measurements of the inlet and outlet temperatures) was performed. The average temperature of the heater and the average temperature of the Pyrex cover were used to calculate the heat losses to ambient. The heat losses, N_3, due to free convection and radiation were calculated and then the power due to the axial heat flux, N_2, was determined using Eq. (1). It is important to stress that the heat losses N_3 from the silicon chip and water in the channels were only a small fraction—between 1% and 2% of the total energy input from the heater (Table 1).

The heated area, A, was defined as the projected area equal to the heater plate area (1×1 cm) [15,16]. The mass velocity was calculated as $\dot{m} = Q\rho/F$, where Q is the volumetric flow rate, ρ is the fluid density, and F is the overall cross-section area of the micro-channels. The Reynolds number was calculated as $Re = ud_{\mathrm{h}}/v$, where u is the bulk flow velocity in the micro-channel, d_{h} is hydraulic diameter. The mean water temperature was used to determine the physical properties of the water. The following procedure was used to determine the wall temperature of the micro-channel from an infrared image of the heater. The straight lines on the bottom of the heated module corresponding to the streamwise axes of each micro-channel were determined using the special image-processing software. Along each line, the temperature on the heated wall was determined. Temperatures shown in the present work are given for the channel, placed at the central part of the chip.

3. Numerical simulations

Three-dimensional numerical model was developed for the computer code CFX5 and numerical results were compared with experimental ones. Heat transfer equations were solved simultaneously in the fluid and in the solid phase. The calculation models are shown in Fig. 2a–c. First a simple "Test model": triangular micro-channel heated from all three sides was used to verify the CFX code with analytical results (Fig. 2a). The second model was a "Complete model" of the experimental device that includes the silicon chip with 17 micro-channels and with steel inlet and outlet collectors (Fig. 2b). The third model was "Reduced model" that represented a single channel from the experiments (Fig. 2c). Most of the results were finally calculated with the "Reduced model". The calculations were carried out for only half of the channel due to the symmetry of the domain.

3.1. Analysis

Physical model, equations, and boundary conditions. Consider a three-dimensional models of cooling channels shown in Fig. 2a and c ("Test model" and "Reduced model"), and a model of complete cooling device, which includes steel inlet and outlet collectors shown in Fig. 2b ("Complete model"). The models were described with the following assumptions:

Table 1
Summary of measured and calculated data

Case	Experiment									CFX simulation			
	$\dot{m}$ (g/s)	$N = U * I$ (W)	$T_{\text{f-in}}$ (K)	T_{CHIP} (K), $L = 10$ mm				$T_{\text{f-out}}$ (K)	N_{1-E} (W)	N (W)	N_1 (W)	N_2 (W)	N_3 (W)
				$x/L = 0.2$	$x/L = 0.4$	$x/L = 0.6$	$x/L = 0.8$						
1.1	0.0088	0.918	304.9	310.3	311	311.3	311.4	308.1	0.12	0.92	0.19	0.72	0.01
1.2	0.0088	2.187	312.8	326.2	328.7	329.7	329.7	321.8	0.33	2.18	0.50	1.65	0.03
1.3	0.0088	3.007	318	339	341.9	342.4	341.4	331.9	0.51	3.00	0.75	2.20	0.05
2.1	0.0178	1.342	304.4	310.1	311.3	312.3	312.8	310.1	0.43	1.34	0.52	0.80	0.02
2.2	0.0178	3.366	308	322.6	325.4	327.3	327.4	321.6	1.02	3.37	1.28	2.10	0.05
2.3	0.0178	5.000	314.7	335.8	340.1	342.6	342.9	335.3	1.54	5.00	1.82	3.10	0.08
3.1	0.0356	2.816	301.3	307.4	309.4	311	311.7	309.4	1.21	2.81	1.19	1.60	0.02
3.2	0.0356	5.676	305.6	318	321.9	324.9	326.7	321.9	2.44	5.67	2.63	3.00	0.04
3.3	0.0356	8.424	309.6	331.3	336.8	340.7	342.5	335.6	3.89	8.42	3.96	4.40	0.06
4.1	0.0711	5.160	300.5	306.8	309.5	311.5	312.2	309.7	2.75	5.16	2.74	2.40	0.02
4.2	0.0711	10.740	303.2	317.7	322.2	326.1	328.4	333.9	6.18	10.75	6.01	4.70	0.04
4.3	0.0711	15.984	306.2	327.1	334.8	340.3	342.9	337.4	9.32	15.49	8.41	7.01	0.07
5.1	0.1422	8.960	299.3	307.1	309.9	312	312.9	308.7	5.61	8.43	5.01	3.40	0.02
5.2	0.1422	17.556	302.4	317.3	322.5	326.4	328.4	320.6	10.87	16.86	10.62	6.20	0.04
5.3	0.1422	27.354	304.2	326.2	334.4	340.7	344	332.2	16.72	25.30	15.73	9.51	0.06

N–electric power of the heater, N_1–power transferred from the silicon to the fluid in the micro-channels: N_{1-E}–estimated from experimental data and Eq. (3), N_1–corrected number used in simulations, N_2–power transferred into the collector by heat conductivity, N_3–heat losses from the chip.

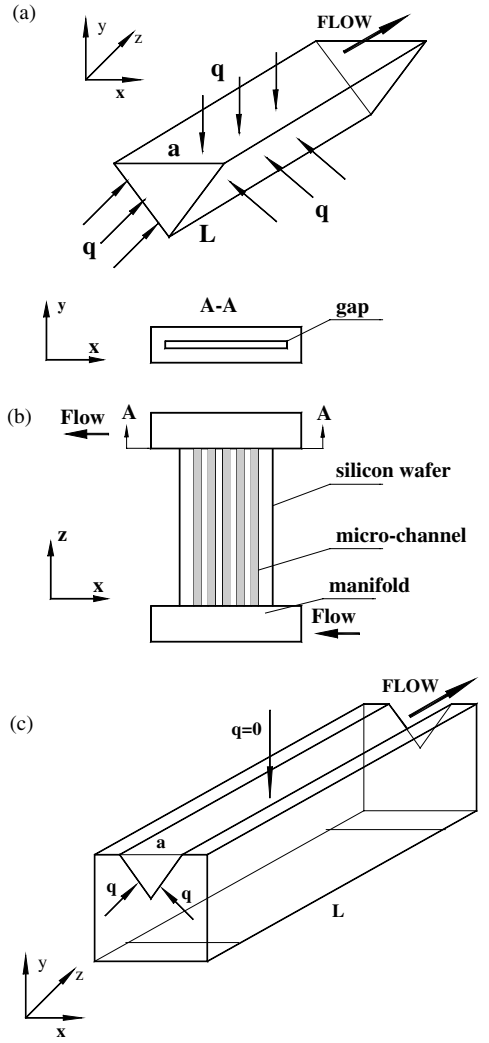

Fig. 2. Calculation models: (a) test model, (b) complete model and (c) reduced model.

- the transport processes are considered to be steady-state and three-dimensional,
- the flow is incompressible and laminar,
- thermal radiation into the channels is neglected in comparison to the convection,
- the physical properties are not temperature dependent,
- properties of silicon, steel, and water at room temperature are specified for the chip, collectors, and the fluid, respectively (steel properties relevant only for "Complete model"),
- pyrex layer and copper heater were not explicitly modelled.

Under the stated assumptions, the conservation equations are:

conservation of mass (continuity)

$$\nabla \cdot \vec{u} = 0 \tag{4}$$

conservation of momentum

$$-\nabla(\vec{u}\vec{u}) + \nu\nabla^2\vec{u} - \nabla p/\rho = 0 \tag{5}$$

conservation of energy for the fluid

$$-\nabla(\vec{u}T) + \alpha_f\nabla^2 T = 0 \tag{6}$$

conservation of energy for the solid (silicon and steel)

$$\alpha_s\nabla^2 T = 0 \tag{7}$$

Boundary conditions for the water velocity, pressure and temperature:

- no-slip boundary conditions at all solid walls,
- constant mass flow rate at the inlet surface (see Table 1),
- constant pressure of 1 bar was specified as a boundary condition at the outlet surface,
- temperature boundary conditions are: constant temperature ($T = 298$ K) at the inlet and $\mathrm{d}T/\mathrm{d}z = 0$ at the outlet,
- at the fluid-pyrex boundary (top of the chip) the heat losses were specified as $q_{fp} = -h(T_f - T_a)$, with heat transfer coefficient $h = 10$ W/(m^2 K),
- the continuity of the temperature and heat flux is automatically used in the CFX code as conjugate boundary conditions to couple the energy equations for the fluid and solid phases.

Silicon and steel temperature boundary conditions:

- at all outer boundaries of the chip and collectors the heat losses were specified as $q_{sl} = -h(T_f - T_a)$, with heat transfer coefficient $h = 10$ W/(m^2 K). The approximation of constant heat transfer coefficient is close enough due to the relatively minor importance of the heat losses (last column in Table 1).
- thin copper heater was modelled as a boundary condition with specified heat flux into the silicon.
- zero thermal resistance was assumed between the silicon chip and the steel collectors boundaries (only in "Complete model" where collectors are present) with continuous temperature and heat flux.

3.2. Model validation

Test model. The ability of the CFX code to properly simulate the conjugate heat transfer in a single micro-channel with equilateral triangle cross-section shown in Fig. 2a was tested as the first step. The model assumed laminar flow of water at similar Reynolds numbers as in the micro-channel cooling experiment, heated by a layer of highly conductive silicon from all three sides. Eqs.

(1)–(4) were solved in the equilateral triangular micro-channel with triangle side of 0.31 mm and channel length 10 mm shown in Fig. 2a. Constant mass flow rate was specified as an inlet boundary condition (0.0107 and 0.172 g/s at $Re = 5$ and 87, respectively) and constant ambient pressure as an outlet boundary condition. External boundaries of the silicon layer were heated with a constant heat flux (2800 and 42,500 W/m^2 at $Re = 5$ and 87, respectively), except the small inlet and outlet silicon boundaries, which were assumed to be adiabatic. Theoretical Nusselt number for the fully developed laminar flow through the channel of equilateral triangle cross-section, heated from all sides with material of infinitely high conductivity is 3.111 [19]. Results were calculated with the fluid volume and the silicon heater volume discretized in 0.95 and 2.85 million tetrahedrons, respectively (numbers are for half of the channel shown in Fig. 2a as the symmetry of the problem was taken into account). Steady-state solution of the laminar Navier–Stokes equations with conjugate heat transfer calculation was found with CFX in the corners of the tetrahedrons (called nodes in CFX: number of nodes was 0.18 and 0.55 million in fluid and solid, respectively) with iterative procedure that took a few hundreds steps. Average Nusselt number in the test pipe calculated by CFX was in expected agreement with theoretical value 3.111. We obtained $Nu = 3.11$ and 3.19 at similar Reynolds numbers as in the experiment $Re = 5$ and 87, respectively.

Complete model. A model of complete cooling device with silicon chip, inlet and outlet steel collectors and water flowing through is shown in Fig. 2b. As already mentioned the grid density of the "Complete model" is far too rough to accurately capture the details of the heat transfer inside the micro-channels. The limitation was imposed by the computer (4×400 MHz, 4GB RAM) as the "Complete model" consisted of almost 3 million tetrahedrons. The calculations of the silicon chip in the "Complete model" were carried out for experimental conditions of the case 1.3 from Table 1.

The results and the temperature field predicted by the "Complete model", shown in Fig. 3 can be compared with experimental results and numerical results of "Reduced model" in Table 1. Two main features are seen in the Fig. 3, which shows the temperature field for the experimental case 1.3 (see Table 1) in the plane of the heater (in silicon, water, and steel domains):

(i) Significant temperature gradients exist in the inlet and outlet collectors. It means that the temperatures measured by the thermocouples approximately in the center of the inlet and outlet collectors are up to a few degrees lower than the actual temperatures at the inlet and outlet of the micro-channels. These temperatures cannot be used to accurately calculate the integral heat transfer rate N_1 inside the chip with Eq. (3). Numerical calculations show that this effect is more important at low velocity cases 1.1–3.3, while it is of minor importance for test cases 4.1–5.3, where Eq. (3) was quite

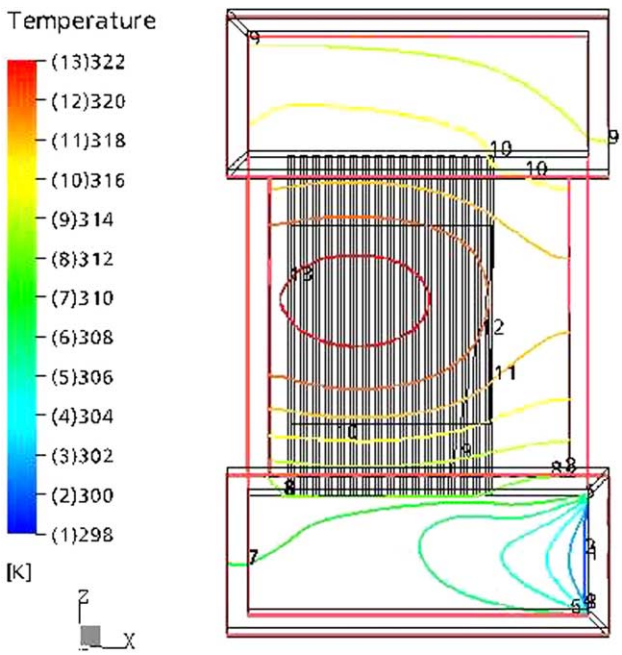

Fig. 3. Temperature field predicted by the "Complete model".

accurate (see Table 1 for values of N_{1-E} estimated from experiment and value N_1 used in simulations).

(ii) Measured temperature differences between the water in the inlet and outlet collectors are higher than predicted by the "Complete model". It means that the heat transfer rate N_2 from the silicon to the steel collectors—cannot be accurately calculated with the "Complete model" due to unknown thermal resistance between the silicon and collectors.

Reduced model. Due to the insufficient information about the axial heat conduction between the silicon chip and steel collectors, it was decided to make a complete set of simulations with a "Reduced model" shown in Fig. 2c. Model represents a single micro-channel and a corresponding slice of the silicon with symmetric boundary conditions applied on the left and right side of the domain. Heat losses in the left ($-x$) and right ($+x$) directions are neglected assuming that the simulated channel is one of the channels in the middle and not one of the side channels. On the topside the heat losses were prescribed as a boundary condition. Heat losses are prescribed as solid boundary conditions also at the unheated parts of the bottom.

Estimate of the inlet/outlet axial heat flux in the Reduced model. As already mentioned, the main unknowns in the experiments and in the numerical model are the two heat fluxes from the silicon chip via heat conduction into the steel inlet and outlet collectors. These two heat fluxes turn out to be crucial for successful simulation of the experiment.

We estimate and tune the axial heat fluxes at the inlet and outlet boundary of the "Reduced model". Half of the N_2 heat transfer rate was prescribed as the boundary condition at the inlet and half as the boundary condition at the outlet side of the silicon chip in "Reduced model". Results of the simulations were compared with experiments and heat fluxes at the inlet and outlet ends were modified accordingly. Simulations presented in Table 1 showed that the N_1 heat transfer at higher velocities (cases 4.1–4.3, 5.1–5.3) is slightly too high when calculated with Eq. (3). Accordingly, repeated simulations were performed with 0–20% reduced values of N_1 heat transfer (see columns N_{1-E} and N_1 in the Table 1). Low velocity cases show that the N_1 heat transfer rate of Eq. (3) must be increased between 5% (case 3.3) and 80% (case 1.1) to obtain agreement with experimental results. Results for each case in the next section were obtained with 2–3 simulations with "Reduced model", where the N_1 heat transfer rates were consecutively corrected.

We performed a few test runs for some of the cases where the N_2 heat transfer was not split in 50:50 ratio between inlet and outlet side of the silicon chip, but in 60:40 and 40:60 ratio. However, as we compared the results we concluded that 50:50 splitting is not very far from the actual splitting.

4. Results and discussion

Temperature distribution. The bulk water temperature and wall temperature on the inner heated wall of the triangular channel is shown in Fig. 4a–c. In these figures solid lines, dotted lines and points represent numerical results of the heated wall temperature, bulk water temperature and experimental results of the temperature on the heater. Experimental data shown in Fig. 4a–c are taken from Table 1. Appropriate constant values were added to all measured temperatures to shift the temperature of the inlet water to 298 K and enable comparison shown in Fig. 4a–c (for example: experimental data shown in Fig. 4a are experimental values for the case 3.1 in Table 1 decreased by 3.3K). A good agreement is seen between measured and predicted temperatures. Some interesting features are readily observed in the figures. Both temperatures do not change linearly along the longitudinal z-direction. In fact, a linear temperature rise cannot be regarded as a good approximation for both temperatures. Moreover, both water and heated surface temperatures do not change monotonously. There are significant changes in the temperature gradient in the z-direction. At some values of z the temperature gradients change sign. This value depends on the Reynolds number and shifts to the channel outlet with an increase in Re. This trend was observed for all flow and heat flux conditions of the present study. From Fig. 4a–c one can see that at certain part of the channel the temperature of the heated inner channel wall is lower than that of the water bulk temperature.

The results obtained in the present study differ significantly from those presented by Qu and Mudawar [13,14]. The three-dimensional fluid flow and heat transfer in a rectangular micro-channel heat sink was analyzed numerically by Qu and Mudawar [14] using water as the cooling fluid. The heat sink consists of 1 cm^2 silicon wafer. The micro-channels have a width of 57 μm, a depth of 180 μm, and are separated by a 43 μm wall. The Reynolds number was $Re = 140$. For the thermal boundary conditions, adiabatic boundary conditions were applied to all the boundaries of the solid region except the heat sink top wall, where a constant heat flux is assumed. At the channel inlet, the liquid temperature was equal to a given constant inlet temperature. The flow is assumed thermally fully developed at the thermal outlet, $d^2T/dz^2 = 0$. One can see that Reynolds number and thermal boundary conditions at the inlet and outlet of the test section are quite different from those used in our study. Qu and Muddwar [14] presented results for single channel. We considered heat exchanger that contains a number of parallel micro-channels connected with inlet and outlet manifolds.

In these studies the effect of inlet and outlet collectors was not considered. The results [13,14] indicated very slight changes in the temperature gradient in the

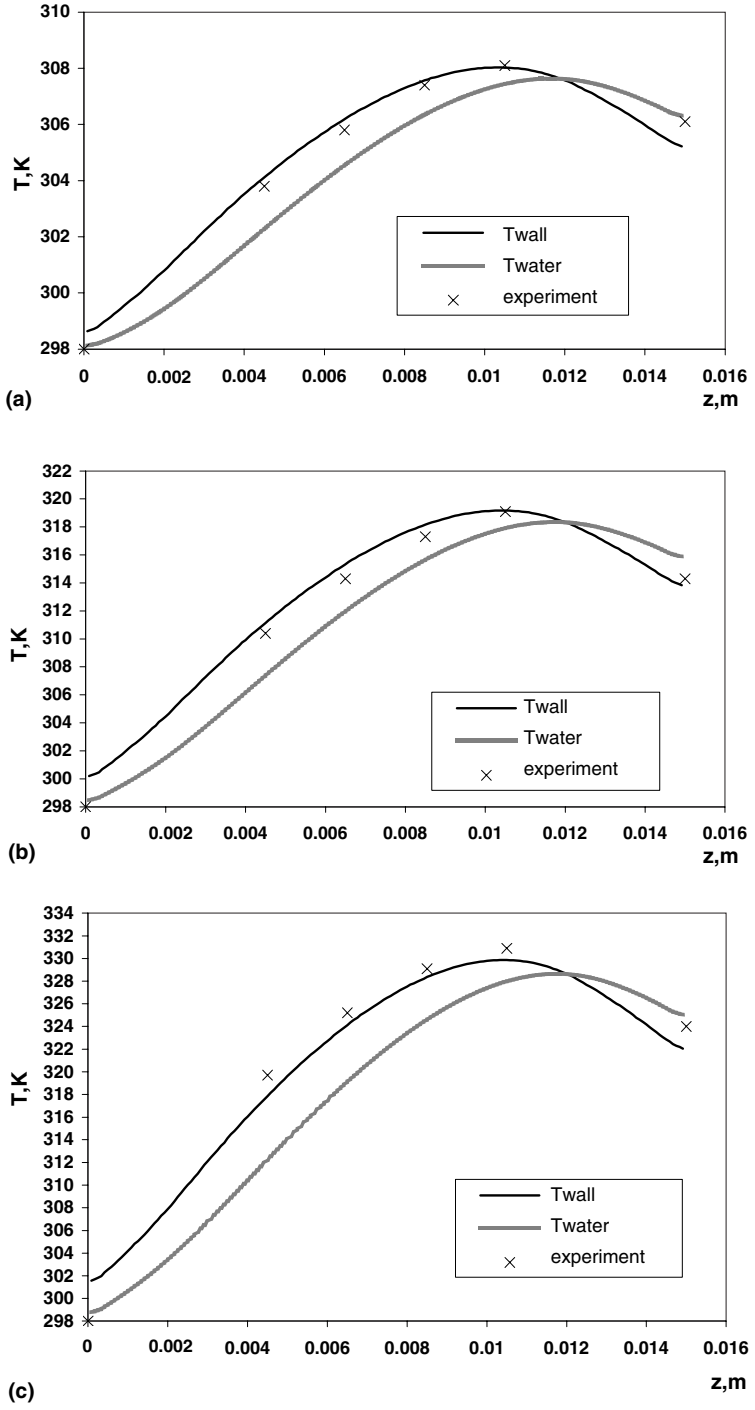

Fig. 4. Average water and silicon temperature distributions: $\dot{m} = 0.0356$ g/s, (a) $N = 2.816$ W, (b) $N = 5.676$ W and (c) $N = 8.424$ W.

streamwise direction at the channel wall. We discuss this point with regard to design of the test module. Consider a collection of parallel micro-channels embedded in a silicon wafer. A coolant flows in each channel, absorbing heat from the walls. These channels were etched directly in the test module. Silicon wafer used for test module, has a high thermal conductivity ($k = 149$ W/m K, about 1/3 of copper thermal conductivity). High conductivity of silicon and steel have given rise to high axial heat flux. Depending on the

Reynolds number, axial heat flux causes temperature distribution on the heated channel wall. In some cases (low collector temperature, low *Re*) the temperature of the heated wall at a given cross-section might be less than bulk temperature of the coolant.

The typical temperature contour maps for the case 1.1 (Table 1) are shown in Fig. 5a for cross-section at $z = 0.002$ m and in Fig. 5b for cross-section at $z = 0.012$ m. Taking advantage of symmetry, we present half of a channel and the surrounding solid. It can be seen from the figure that the boundary between the solid and the fluid is not clearly visible due to a small change in the wall normal temperature gradient at the interface. Due to the high conductivity and small thickness (about 1 μm) of the copper film heater, the temperature gradient over it is so small that it can be regarded as isothermal at each x–y cross-section. Therefore, it is safe to use the heater temperature to represent the temperature of silicon wafer at $y = 0$. Due to the silicon's high thermal conductivity, the temperature gradient in the silicon wafer is very small and the temperature field is also close to an isothermal one at each x–y cross-section. The temperature variation in the fluid is clearly visible. Note that for cross-section at $z = 0.002$ m the water temperature is lower than temperature of silicon wafer, for cross-section at $z = 0.012$ m the opposite trend takes place. This implies that at low Reynolds number the axial heat conduction in the silicon close to the outlet collectors is more important for heat transport in heat think.

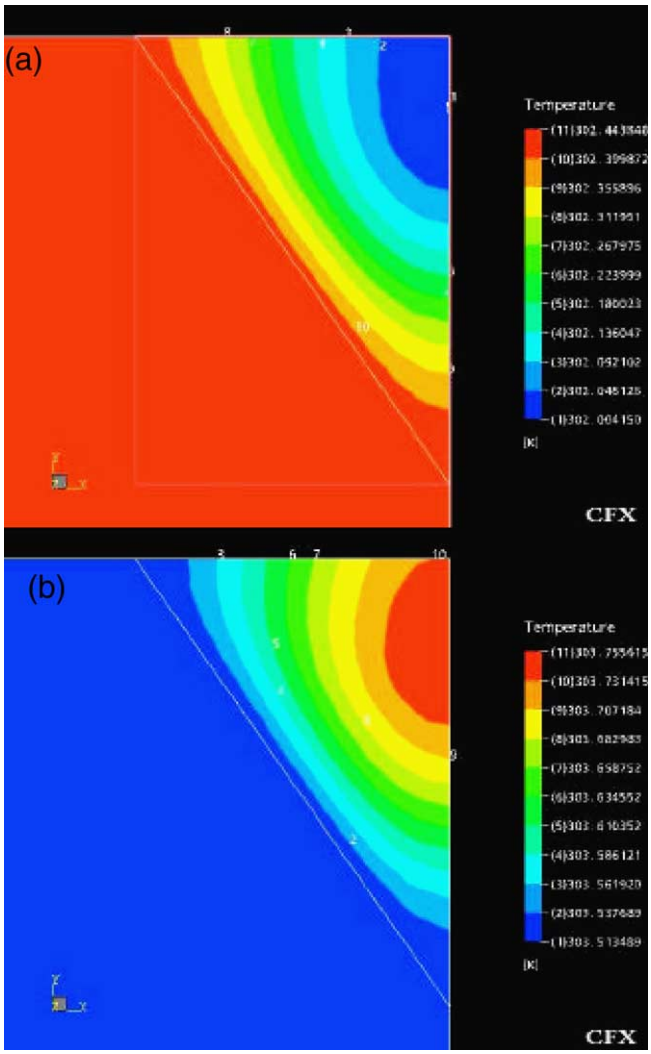

Fig. 5. Temperature contours of the "Reduced model" for the case: $m = 0.0088$ g/s, $N = 0.918$ W (a) $z = 2$ mm from the inlet and (b) $z = 12$ mm from the inlet.

Effect of axial heat conduction in the channel wall. Fig. 6a–c shows the numerical results of the silicon wafer cross-section average value of axial heat flux in the streamwise direction. The axial heat flux has the minimum negative value at the distance about 0.002 m from the inlet and it remains negative up to distance about 0.01 m from the inlet (i.e. acts in the direction opposite to the flow). Then axial heat flux becomes positive, i.e. acts in the flow direction. Qu and Mudawar [13,14], Fedorov and Viskanta [20] did not observe such a phenomenon since the design of heat sink used in their numerical analysis did not include inlet and outlet collectors.

Wall normal heat flux. The longitudinal distributions of the silicon-fluid wall normal heat fluxes averaged in the x–y planes are presented in Fig. 7a–c. The heat fluxes are taken to be positive if they are directed from the solid to the fluid, and negative, otherwise. The local

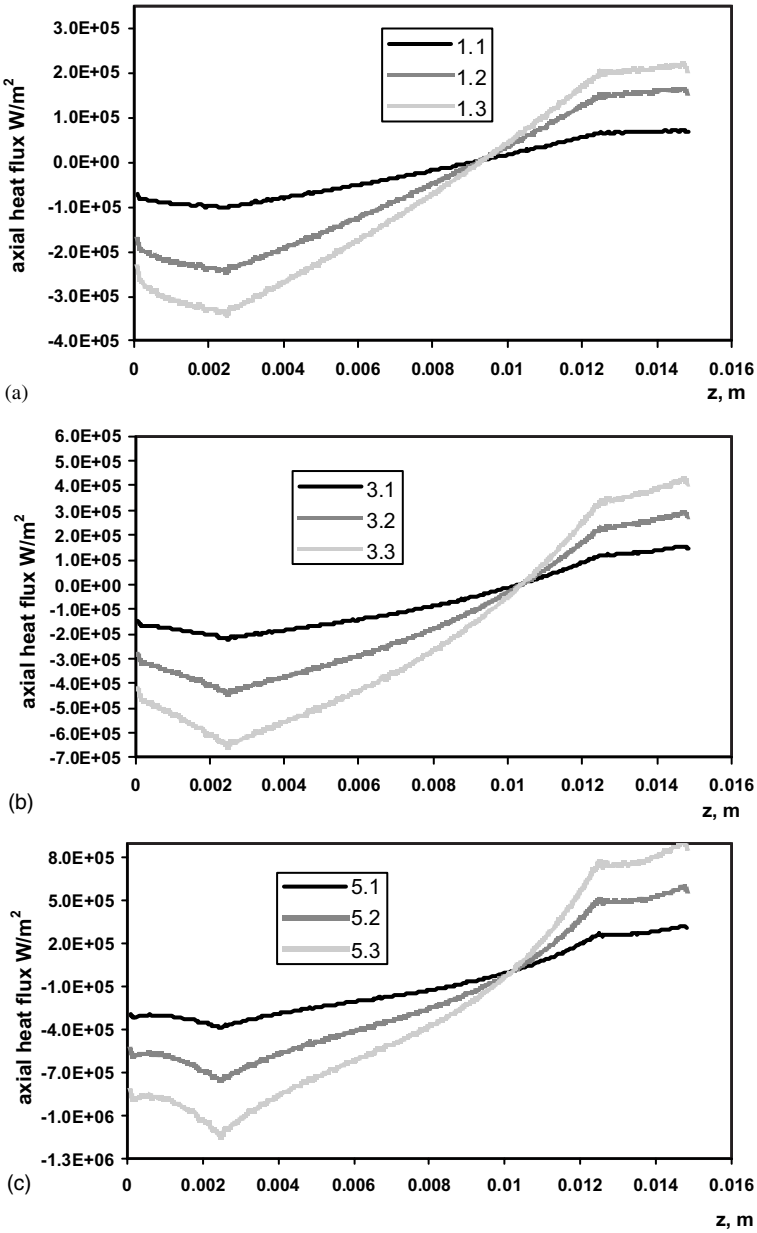

Fig. 6. Axial heat flux distribution: (a) $\dot{m} = 0.0088$ g/s, 1.1: $N = 0.918$ W, 1.2: $N = 2.187$ W, 1.3: $N = 3.007$ W; (b) $\dot{m} = 0.0356$ g/s, 3.1: $N = 2.816$ W, 3.2: $N = 5.676$ W, 3.3: $N = 8.424$ W and (c) $m = 0.142$ g/s, 5.1: $N = 8.960$ W, 5.2: $N = 17.556$ W, 5.3: $N = 27.354$ W.

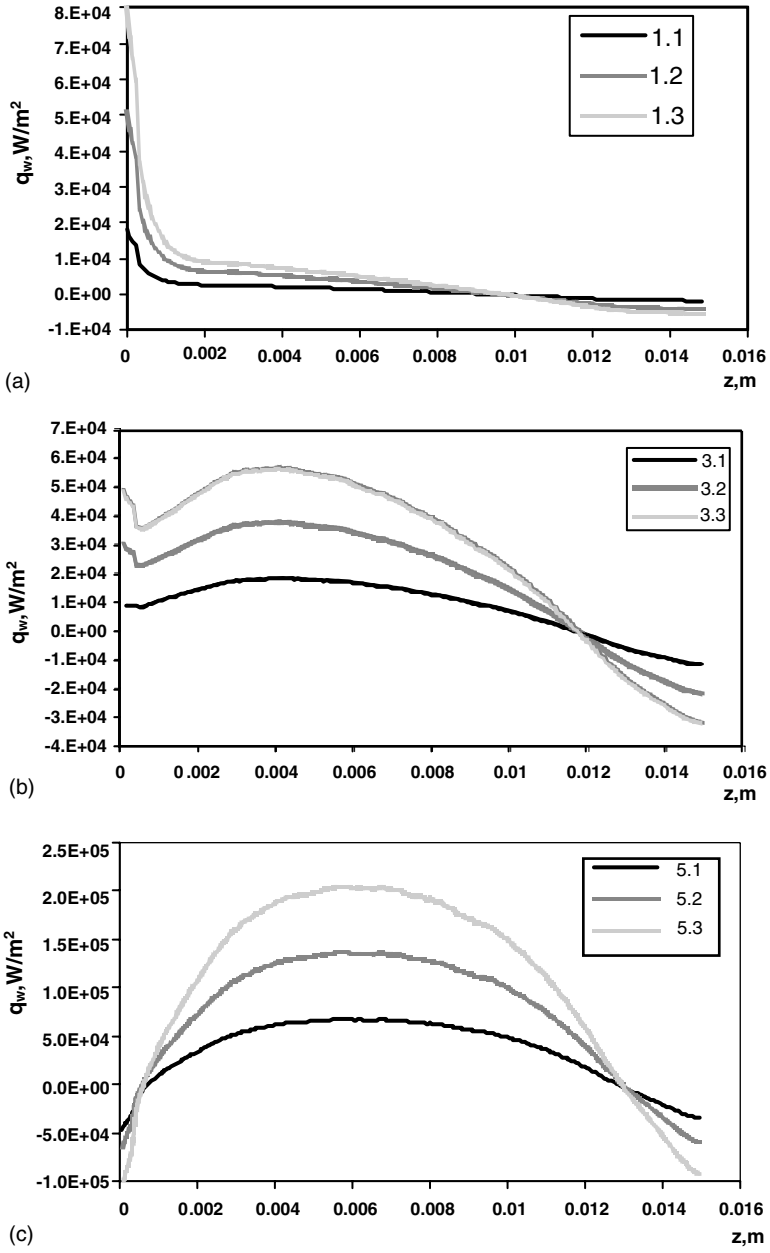

Fig. 7. Wall normal heat flux distribution in the silicon chip: the legend is the same as in Fig. 6.

heat fluxes are the greatest in the inlet portion of the channel, and they decrease rapidly in the longitudinal z-direction. The direction and the magnitude of the negative heat flux depends on relation between the two thermal resistance's: the first defines the heat transport from the wall through the boundary layer to the fluid core, and the second one quantifies the possibility of heat transport trough silicon substrate. The importance of the second alternative pathway for the heat transfer can be truly appreciated only in three-dimensional conjugate heat transfer problem. The thermal wall boundary conditions have a dominant role in such a problem.

Nusselt number. Numerical predictions of local Nusselt number variation in the streamwise direction are plotted in Fig. 8a–c for Reynolds numbers ranged from $Re_{in} = 3.2$ to 84 and different values of heat flux applied at the heater. As indicated by Incropera and De Witt [23] the thermal entry length of a circular tube may be calculated from

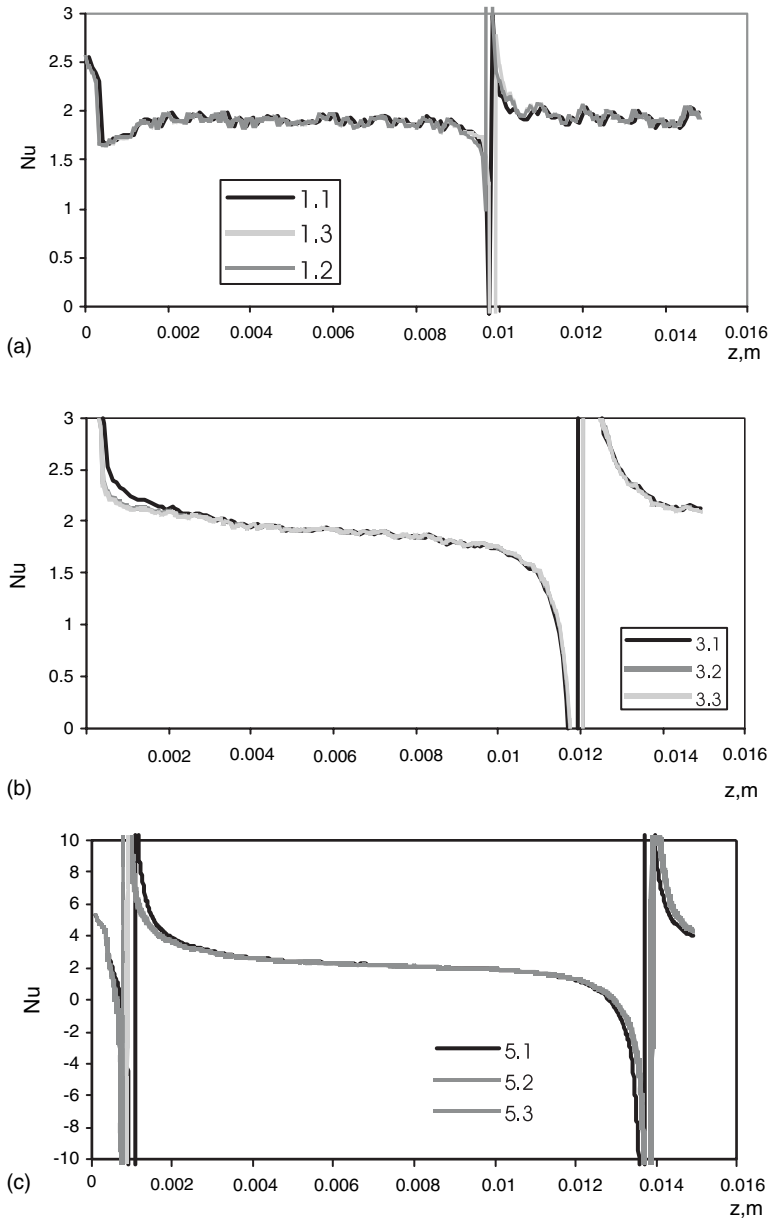

Fig. 8. Axial distribution of Nusselt number in the chip: the legend is the same as in Fig. 6.

$$L_{\mathrm{th}} = 0.05 Re Pr d \tag{5}$$

For the triangular channels the thermal entry lengths can be estimated by replacing the tube diameter with the hydraulic diameter $d_{\mathrm{h}} = 160$ μm. The Prandtl number is $Pr = 4.9$, and the thermal entry lengths are 0.13 and 3.3 mm for $Re = 3.2$ and 84, respectively. In all figures the behaviour of Nusselt numbers has a singular point. At this point the difference between temperature at the inner wall of the channel and bulk water temperature becomes negative and the wall normal heat flux changes the sign and is directed from the fluid to the wall. The singular point shifts closer to the channel outlet with increase in Reynolds number.

The results of the present study are different from numerical calculations carried out for higher Reynolds numbers [13,14]. Qu and Mudawar [13,14] showed that the change of temperature gradient along the flow direction at the channel exit is very small even for very large Reynolds numbers. They assumed that at the channel inlet and outlet the absence of axial heat flux takes place.

The axial heat flux affects the temperature of the heated wall and bulk fluid temperature distribution along the flow direction. It is important to mention that in [10,12] the bulk temperature could not be measured inside the micro-pipe but was interpolated between temperatures that were measured at the inlet and outlet collectors of experimental set-up. From their understanding of the physics of the problem the authors [10,12] assumed a linear interpolation to be adequate. All experimental data fall below the values predicted by the numerical analysis. It was assumed that deviation between determined the experimentally determined Nusselt number and that predicted by the numerical calculations might be caused by the surface roughness [10,12]. A roughness-viscosity model was applied to interpret the experimental results. This point was checked in our experiments. Assuming that the surface roughness causes the effect of viscous dissipation we measured the water temperature at the inlet and outlet collector without heating, i.e. the electrical current was not applied to the heater. These experiments were carried out in the range $Re = 3.2$–84 and showed that the water temperature in the inlet collector did not differ from that in the outlet collector. With a critical view on the experimental test-section in [10] the axial heat conduction in silicon substrate may be identified as crucial. Herwig and Hausner [18] demonstrated the axial heat conduction should explain Tso and Mahulikar's [12] results in a conventional manner (with no need to have resource to special micro-effects).

5. Conclusions

Experimental and numerical analysis were performed to evaluate heat transfer characteristics of water flowing through triangular silicon micro-channels with hydraulic diameter of 160 μm in the range of Reynolds number $Re = 3.2$–64. It was shown that as the bulk water temperature, as well as the temperature of the heated wall, do not change linearly along the channel. The experimental results of temperature distribution on the heated wall agree with the numerical predictions.

Both water and heated surface temperatures do not change monotonously. There are significant changes in the temperature gradient in the flow direction. Close to the channel outlet the temperature gradients change the sign. This value depends on Reynolds number and shifts to the channel outlet with increase in Re. The non-monotonous behaviour of fluid and heated wall temperatures is due to high values of axial heat fluxes in the silicon wafer.

The axial heat flux has a maximum near the inlet collector and decreases in the flow direction up to zero. In this region it remains negative (i.e. it acts in direction opposite to the flow). Then axial heat flux becomes positive, i.e. it acts in the flow direction. In this case the wall temperature decreases and the heat is transferred from the fluid to the silicon wafer.

The behaviour of the Nusselt number along the channel has a singular point. At this point, the difference between the temperatures on the wall and the bulk water becomes negative and the flux changes the sign and is directed from the fluid to the wall. The singular point shifts closer to the channel outlet with an increase of the Reynolds number.

It was shown that under conditions of the present study the dissipation effects can be neglected and the heat transfer may be described by conventional Navier–Stokes and energy equations as a common basis.

Acknowledgements

This research was supported by the Fund for Promotion of Research at the Technion. A. Mosayk is supported by a joint grant from the Center for Absorption in Science of the Ministry of Immigrant Absorption and the Committee for Planning and Budgeting of the Council for Higher Education under the framework of the KAMEA PROGRAM, and E. Pogrebnyak was supported by the Center for Absorption in Science, Ministry of Immigrant Absorption State of Israel.

I. Tiselj and B. Mavko were supported by the Ministry of Education, Science and Sport of the Republic of Slovenia.

References

[1] C.B. Sobhan, S.V. Garimella, A comparative analysis of studies on heat transfer and fluid flow in microchannels, Microscale Thermophys. Eng. 5 (2001) 293–311.
[2] S.B. Choi, R.R. Barren, R.Q. Warrington, Fluid flow and heat transfer in micro-tubes, ASME DSC 40 (1991) 89–93.
[3] X.F. Peng, B.X. Wang, Forced convection and flow boiling heat transfer for liquid flowing through microchannels, Int. J. Heat Mass Transfer 36 (1993) 3421–3427.
[4] A. Weisberg, H.H. Bau, J. Zemel, Analysis of microchannels for integrated cooling, Int. J. Heat Mass Transfer 35 (1992) 2465–2474.
[5] M.B. Bowers, I. Mudawar, High flux boiling in low flow rate, low pressure drop mini-channel and microchannel heat sinks, Int. J. Heat Mass Transfer 37 (1994) 321–332.
[6] B.X. Wang, X.F. Peng, Experimental investigation of liquid forced-convection heat transfer through microchannels, Int. J. Heat Mass Transfer 37 (1994) 73–82.
[7] R.L. Webb, M. Zhang, Heat transfer and friction in small diameter channels, Microscale Thermophys. Eng. 2 (1998) 189–202.
[8] P.Y. Wu, W.A. Little, Measurement of the heat transfer characteristics of gas flow in fine channel heat exchangers

used for micro-miniature refrigerators, Criogenics 23 (1984) 415–4209.
[9] X.F. Peng, G.P. Peterson, The effect of thermofluid and geometrical parameters on convection of liquids through rectangular microchannels, Int. J. Heat Mass Transfer 38 (1995) 755–758.
[10] W. Qu, Gh.M. Mala, D. Li, Heat transfer for water in trapezoidal silicon micro-channels, Int. J. Heat Mass Transfer 43 (2000) 3925–3936.
[11] C.P. Tso, S.P. Mahulikar, The use of the Brinkman number for single phase forced convective heat transfer in microchannels, Int. J. Heat Mass Transfer 41 (1998) 1759–1769.
[12] C.P. Tso, S.P. Mahulikar, Experimental verification of the role of Brinkman number in microchannels using local parameters, Int. J. Heat Mass Transfer 43 (2000) 1837–1849.
[13] W. Qu, I. Mudawar, Experimental and numerical study of pressure drop and heat transfer in a single-phase micro-channel heat sink, Int. J. Heat Mass Transfer 45 (2002) 2549–2565.
[14] W. Qu, I. Mudawar, Analysis of three-dimensional heat transfer in micro-channel heat sinks, Int. J. Heat Mass Transfer 45 (2002) 3973–3985.
[15] M. Gad-el-Hak, The fluid mechanics of micro-devices—The Freemen Scholar Lecture, J. Fluid Eng. 121 (1999) 5–33.
[16] S.S. Mehendale, A.M. Jacobi, R.K. Shah, Heat exchangers at micro- and meso-scales, in: Proceedings of International Conference on Compact Heat Exchangers and Enhance Technology for the Process Industries, Banff, Canada, 1999, pp. 55–74.
[17] R. Palm, Heat transfer in micro-channels, Microscale Thermophys. Eng. 5 (2001) 155–175.
[18] H. Herwig, O. Hausner, Critical view on "new results in micro-fluid mechanics": an example, Int. J. Heat Mass Transfer 46 (2003) 935–937.
[19] R.K. Shah, A.L. London, Laminar flow forced convection in ducts, in: T.F. Irvine, J.P. Hartnett (Eds.), Advances in Heat Transfer, Supplement 1, Academic Press, New York, San Francisco, London, 1978.
[20] A.G. Fedorov, R. Viskanta, Three-dimensional conjugate heat transfer in the micro-channel heat sink for electronic packaging, Int. J. Heat Mass Transfer 43 (2000) 399–415.
[21] G. Hetsroni, A. Mosyak, Z. Segal, Nonuniform temperature distribution in electronic devices cooled by flow in parallel micro-channels, IEEE Trans. Components Packag. Technol. 24 (2001) 16–23.
[22] G. Hetsroni, A. Mosyak, Z. Segal, G. Ziskind, A uniform temperature heat sink for cooling of electronic devices, Int. J. Heat mass Transfer 45 (2002) 3275–3286.
[23] F.P. Incropera, D.P. De Witt, Fundamentals of Heat and Mass Transfer, fourth ed., Wiley, New York, 1996.